



Hopes Beyond PET Recycling: Environmentally Clean and Engineeringly Applicable

Ramin Shamsi^{1,2} · Gity Mir Mohamad Sadeghi¹ · Henri Vahabi^{3,4} · Javad Seyfi⁵ · Reza Sheibani² · Payam Zarrintaj^{6,7,8} · Fouad Laoutid⁹ · Mohammad Reza Saeb^{3,4,8,10} 

Published online: 19 August 2019
© Springer Science+Business Media, LLC, part of Springer Nature 2019

Abstract

Disposal of plastics in the environment has become a core of anxiety in developing countries, while in the developed countries the focus has additionally been placed on design and manufacture of emerging products from plastic wastes—a somewhat vague yet promising horizon. Central to environmental concerns are poly(ethylene terephthalate) (PET) wastes, mainly from post-consumer bottles. Because of a considerable drop in molecular weight in the course of recycling, recycled PETs are not suitable for engineering uses. An efficient yet reasonably green synthesis route is employed here to convert PET wastes into polyurethane, and then carbon nanotubes (CNTs) was added at different levels to obtain nanocomposites with high mechanical properties. The effects of isocyanate (NCO)/hydroxyl (OH) molar ratio and CNTs content on the morphology, physical and mechanical properties were discussed. Chemical/physical crosslink density was calculated from initial slope of stress–strain curves, Mooney–Rivlin plots, strain-hardening modulus, rubbery-plateau storage modulus and swelling data. High tensile strength (300 MPa) and breaking elongation (160%) of polyurethane/CNTs nanocomposites born from PET wastes seemed promising. Microscopic analyses by AFM, SEM, and TEM gave useful information about distribution of CNTs in polyurethane. Lastly, structural changes were correlated to mechanical properties improvement.

Keywords Nanocomposites · PET waste · Polyurethane · CNTs · Recycling

Introduction

The variety and enormous bulk of plastic wastes in the human landscape has become a serious threat to the environment. Such a concern raised the question of choice for

clean disciplines that could principally allow for taking legitimate steps to protect the environment. Plastic wastes are frequently discharged to the environment or landfilled; hence, making smart use of sustainable alternatives to such conventional mistakenly-used solutions remains a confusing

✉ Gity Mir Mohamad Sadeghi
gsadeghi@aut.ac.ir

✉ Mohammad Reza Saeb
saeb-mr@icrc.ac.ir

¹ Department of Polymer Engineering and Color Technology, Amirkabir University of Technology, Tehran, Iran

² Research & Development Center, Marun Petrochemical Company, Mahshahr, Iran

³ Université de Lorraine, Centrale Supélec, LMOPS, 57000 Metz, France

⁴ Laboratoire Matériaux Optiques, Photoniques et Systèmes, Centrale Supélec, Université Paris-Saclay, 57070 Metz, France

⁵ Department of Chemical Engineering, Azad University, Shahrood Branch, P.O. Box 36155-163, Shahrood, Iran

⁶ Polymer Engineering Department, Faculty of Engineering, Urmia University, Urmia, Iran

⁷ Color and Polymer Research Center (CPRC), Amirkabir University of Technology, P.O. Box 15875-4413, Tehran, Iran

⁸ Advanced Materials Group, Iranian Color Society (ICS), P.O. Box 1591637144, Tehran, Iran

⁹ Center of Innovation and Research in Materials & Polymers (CIRMAP), Laboratory of Polymeric and Composite Materials (LPCM), University of Mons UMONS & Materia Nova Research Center, Place du Parc 20, 7000 Mons, Belgium

¹⁰ Department of Resin and Additives, Institute for Color Science and Technology, P.O. Box: 16765-654, Tehran, Iran

implication. For instance, only in developing countries did a cultural paradigm shift take place on the ground of the belief that green strategies will serve the whole community. However, the future-oriented concerns in the developed countries are aimed to dabble in answering further questions on how to manage to get high-quality products from recycled plastic wastes.

Recycling of poly(ethylene terephthalate) (PET) wastes received attention over years in the hope of obtaining invaluable products with acceptable properties [1], but the quality of PET-wastes-driven products was not adequate for engineering uses [2]. Thanks to the coexistence of hard and soft segments that could give rise to a wide range of properties [3], polyurethanes (PUs) were of interest among derivatives obtained from PET wastes [4]. Typically, a number of factors govern physical, chemical, and mechanical properties of PUs, among which hard segment content in the backbone of polymer plays the most vital role in the value of ultimate properties [5–7]. Not surprisingly, chance of success in producing PUs with satisfactory mechanical properties from PET wastes—without mixing the recycled polyols with a high amount of virgin polyol—is quite limited [8]. PUs containing polyol reveal rubber-like behavior at high NCO/OH molar ratios; however, the highest tensile strength achieved was seemingly ca. 8.8 MPa, while elongation at break and modulus took even 320% and 16.67 MPa values, respectively [9].

In a series of papers, we reported on synthesis of PU from post-consumer PET wastes. First, we reported on the synthesis of adhesives and biodegradable PUs [10, 11]. In situ polymerization of PU in the presence of multi-walled carbon nanotubes (CNTs) was then examined [12]. The viscoelastic behavior of the resulting nanocomposites was studied through dynamic mechanical analysis (DMA) in the next work under either frequency or temperature sweep, along with their creep behavior [13, 14]. A combined theoretical/experimental survey on swelling behavior of products revealed substantial changes taking place in PU structure [12, 15], while no report on mechanical behavior of such nanocomposites was published.

In this work, a comprehensive study was performed on PU/CNTs nanocomposites starting from synthesis of polyols from post-consumer PET bottles followed by exploring structure–property relationships. The superiority of mechanical properties observed for nanocomposites born from PET wastes at specified CNTs content was explained on account of semi-theoretical evaluations on changes in the crosslink density (CLD) values. A detailed work was also performed on stress–strain curves, Mooney–Rivlin plots, strain hardening modulus, plateau of storage moduli in the rubbery region. Since the urethane linkage (–NHCOO) is the result of reaction between a hydroxyl group (–OH) of polyol and isocyanate (–NCO) group of diisocyanate, fluctuations

in mechanical properties were correlated with changes in NCO/OH ratio, as monitored by Fourier-transform infrared spectroscopy (FTIR) analyses. The topological changes were imaged using atomic force microscopy (AFM), while scanning electron microscopy (SEM) and transmission electron microscopy (TEM) observations allowed for probe into the microstructural changes in the PUs and PU/CNTs nanocomposites. Dynamic mechanical analysis (DMA) was used to study viscoelastic behavior of samples.

Experimental

Materials

Post-consumed PET bottle wastes were provided by the local market and cut into approximately 1 cm × 1 cm pieces after removal of their caps and labels. The resulting squared samples were washed with detergent and then with methanol to erase adhesives. Adipic acid (AA), dibutyltin dilaurate (DBTDL), hexamethylene diisocyanate (HDI), zinc acetate, dimethyl formamide (DMF), toluene and dimethylacetamide (DMAc) were purchased from Merck Co. (Germany). Moreover, 2-methyl-1,3-propanediol (MPD) was provided by Sigma Aldrich (France). Multi-walled carbon nanotube (CNTs) with hydroxyl content of 3.7 wt%, diameter of 8–15 nm, the length of 50 μm, and 95% purity was purchased from the American Elements Co. (USA). All the reagents were used without further purification.

Synthesis of PUs and PU/CNTs Nanocomposites from PET Wastes

The PET flakes resulting from post-consumer bottle wastes were glycolized to collect polyester diol. PU and PU/CNTs composites were then synthesized in situ according to the procedure illustrated in Fig. 1 [12].

To achieve PU from PET wastes, PET chain scission is required to achieve low-molecular weight PET. To do so, PET wastes in the form of flake were glycolized so as to conduct transesterification of PET in the presence of the MPD in 1:6 molar ratio. The product of PET depolymerization, which is was oligoester (diol) together with AA underwent reaction at a fixed hydroxyl/carboxyl ratio of ca. 2. The synthesis of PU was carried out by exposing the as-synthesized diol with a certain amount of HDI (Fig. 2; Table 1).

The PU/CNTs nanocomposites were synthesized via in situ polymerization using polyester diol, hydroxylated CNTs (0.5 wt% based on polyester diol), DBTDL, DMF as solvent, and different molar ratios of HDI. To enhance the mechanical properties, the samples were post-cured for 1 h at 50 °C and then conditioned for 12 h at 80 °C.

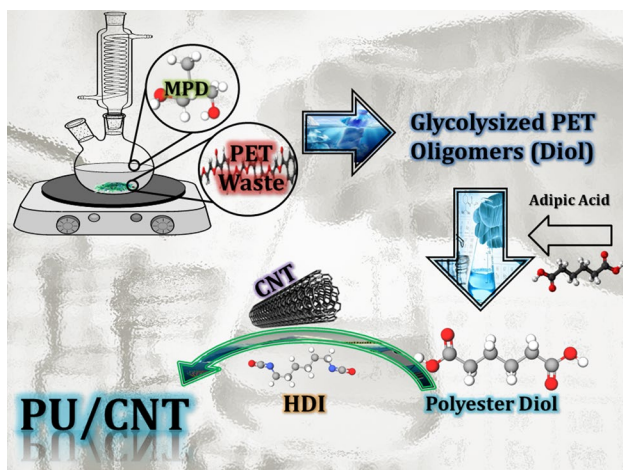


Fig. 1 Synthesis route used to synthesize PU from PET wastes

Characterization of PUs and PU/CNTs Nanocomposites

Chemical Structure Analysis

The hydroxylated CNTs were subjected to FTIR analysis using KBr disc technique on a BRUKER-EQUINOX 55LS FTIR spectrometer. The ATR-FTIR analysis enabled scanning the surface of the synthesized PUs and PU/CNTs samples with a BRUKER-EQUINOX 55LS FTIR spectrometer working in reflection mode. The spectra of the samples were achieved by 20 scans in the wavenumber range $400\text{--}4000\text{ cm}^{-1}$ with a resolution of 2 cm^{-1} .

Physical and Mechanical Properties Analyses

Swelling behavior of the chemically crosslinked samples was studied in toluene and DMAc according a well-documented protocol [12]. The density of the samples was determined based on Archimedes' or buoyancy principle.

The dumbbell-shaped specimens were tested according to ASTM D 1638 with a Cesare Galdabini SPA tensile tester working at extension rate of 50 mm/min. A number of four replicates were used for the sake of reliability of measurements. The Young's modulus, tensile strength, elongation at break, offset yield stress, offset yield strain, modulus of resilience and toughness were all calculated accordingly and reported for each sample.

Shore A hardness values were collected for the PUs and nanocomposites on a Prüfen Messen tester according to the DIN 53505 standard test method.

The abrasion resistance of the PUs and nanocomposites were measured using Prüfen Messen tester according to the standard GB/T 9867-2008. The samples were cut into discs having diameter of 13 mm and tested under the applied force

of 10 N with a rubbing distance of 40 m on the surface of the roll. The abrasion weight loss (%) of each sample was calculated using Eq. (1).

$$\text{Abrasion weight loss (\%)} = \frac{w_1 - w_2}{w_1} \times 100 \quad (1)$$

where, w_1 and w_2 are the sample weights before and after the abrasion test, respectively.

Viscoelastic Behavior Analysis

Dynamic mechanical analysis (DMA) was conducted on a dynamic mechanical analyzer (TT-DMA, Triton technology Co., England) on samples having dimensions $0.25 \times 10 \times 30\text{ mm} \times \text{mm} \times \text{mm}$. A very low displacement (0.01 mm) was applied on PU film samples within the linear viscoelastic region. Analyses were made in the temperature range of $-100\text{ }^\circ\text{C}$ to $150\text{ }^\circ\text{C}$ under nitrogen atmosphere, heating rate of $5\text{ }^\circ\text{C}/\text{min}$ and frequency of 1 Hz. Additional static force (preload) equal to -0.025 N was applied to the samples for the sake of reliability.

Topological and Morphological Analyses

Tapping-mode AFM (USPM, Ambios Technology Corporation, USA) was served to obtain phase data. Samples ($1 \times 1\text{ cm} \times \text{cm}$) were mounted onto a glass plate using a sticky tab. AFM surface scans were taken under ambient conditions ($24 \pm 2\text{ }^\circ\text{C}$). The parameters of testing were adjusted so as to obtain the best image resolution. For each sample, images were collected at different locations to obtain reliable and reproducible images.

The morphology of PUCNT-1.7 and PUCNT-2 nanocomposite samples was observed by SEM (model AIS-2100, Seron Technology, Korea). Nanocomposite samples were fractured within the liquid nitrogen, and then surface-coated with Au for SEM observations. Film samples were prepared by ultramicrotomy with a Leica Ultracut UCT (Leica Mikrosystems GmbH, Vienna, Austria). A diamond knife with cutting edges of 45° was applied to gain smooth sections $50\text{--}80\text{ nm}$ in at a temperature of about $-90\text{ }^\circ\text{C}$. The CNTs within the PU matrix were observed through a high resolution transmission electron microscopy (model EM10C, Zeiss, Germany) operated at an accelerated voltage of 100 keV.

Results and Discussion

As can be seen in Table 1, in contrary to the polyurethanes, formation of chemical crosslinks was impeded in the case of the nanocomposites once the NCO/OH molar ratio was higher than unity. This interesting phenomenon can be

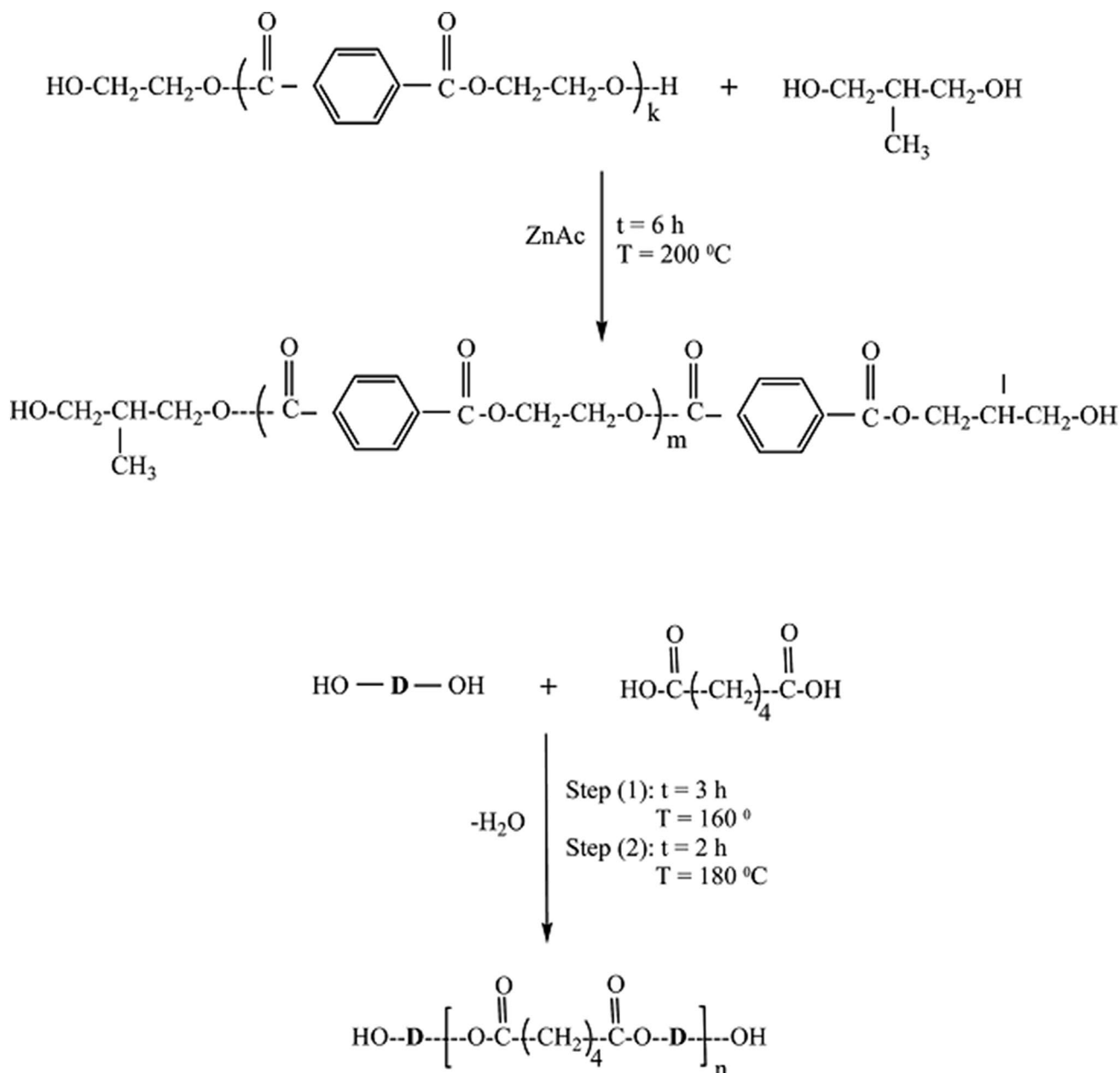


Fig. 2 Possible reaction between PET waste and MPD

Table 1 Physical state and compositions used in the synthesis of the PUs and PU/CNT nanocomposites

Sample	NCO/OH (molar ratio)	CNT (wt%)	Physical state
PU-1	1	–	Thermoplastic
PU-1.7	1.7	–	Thermoset
PU-2	2	–	Thermoset
PUCNT-1	1	0.5	Powder
PUCNT-1.7	1.7	0.5	Thermoplastic
PUCNT-2	2	0.5	Thermoplastic

attributed to the steric hindrance effect of CNTs. However, when the NCO/OH molar ratio was equal to unity, the presence of CNTs and also low amount of diisocyanate in the system prevented the formation of polymer chains which resulted in a powder-like material. Thus, the studies were carried out on the PU-1, PU-1.7, PU-2, PUCNT-1.7 and PUCNT-2 samples.

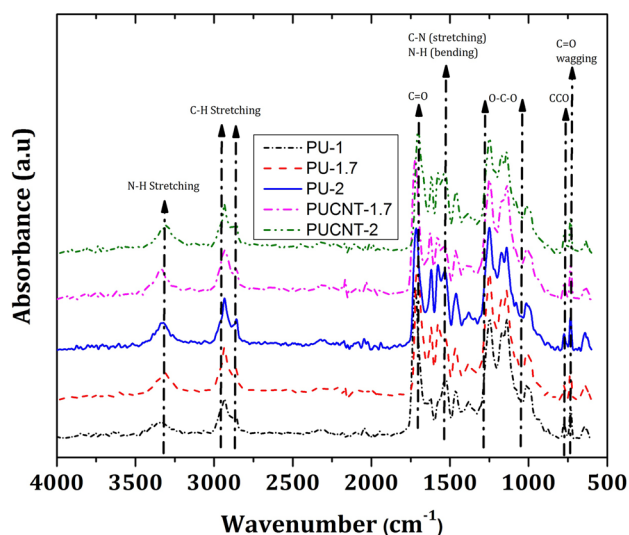


Fig. 3 Absorbance FTIR spectroscopy of the hydroxylated CNTs

FTIR Analysis

FTIR spectrum of the used CNT, shown in Fig. 3, exhibits a broad and strong peak at $\sim 3450\text{ cm}^{-1}$ which is a characteristic of the O–H stretch of hydroxyl group, and it may be attributed to the oscillation of carboxyl groups which originated from the partial oxidation of the surface of CNTs in the course of production. Appearance of a strong peak at $\sim 1740\text{ cm}^{-1}$ indicated formation of carboxylic groups due to the oxidation of some carbon atoms on the surface of CNTs by nitric acid. Peaks at 3745 and 2360 cm^{-1} are related to the free hydroxyl groups and the O–H stretch from strongly hydrogen-bonded –COOH, respectively. Moreover, the peak at $\sim 1540\text{ cm}^{-1}$ is attributed to the carboxylate anion stretch mode [16].

In polyester-based polyurethanes and as-functionalized carbon nanotube based composites, there is a possibility for the formation of hydrogen bonds between different phases of polyurethane and also between CNTs and polyurethane chains [17–20]. The NH group from a hard segment donates a proton, whereas the acceptor group is a carbonyl group in either the hard segment (HDI) or the polyester soft segment. Moreover, in the case of nanocomposites, the functional groups residing on the surface of CNTs could also act as one of the acceptor groups. The analysis of the NH and C=O stretching vibrations also gives valuable information about any possible interactions between the soft and hard segments in PU polymers, and also, the hard segments with CNTs in the polyurethane nanocomposites.

The N–H stretching fundamentals of polyurethanes were observed between 3200 and 3500 cm^{-1} , whereas the region at about 1700 – 1750 cm^{-1} is related to the carbonyl C=O stretching vibrations. In the case of hydrogen bonding, the

stretching vibrations are shifted to lower wavenumbers. In other words, as hydrogen bonding becomes stronger, the frequency shift ($\Delta\nu$) towards the lower wavenumber region would be larger. The $\Delta\nu$ is thus used as an indicator for the existence and intensity of the hydrogen bonding.

FTIR spectra corresponding to the N–H and C=O stretching regions are shown in Fig. 3. The maximum peak frequencies and frequency shifts of the hydrogen bonded N–H stretching modes and also C=O stretching modes for the studied samples are given in Table 2. The frequency shift for N–H stretching region ($\Delta\nu_{\text{NH}}$) and for C=O stretching region ($\Delta\nu_{\text{CO}}$) are defined as Eqs. (2) and (3), respectively.

$$\Delta\nu_{\text{NH}} = \nu_{f,\text{NH}} - \nu_{b,\text{NH}}; \quad \nu_{f,\text{NH}} = 3440\text{ cm}^{-1} \quad (2)$$

$$\Delta\nu_{\text{CO}} = \nu_{f,\text{CO}} - \nu_{b,\text{CO}}; \quad \nu_{f,\text{CO}} = 1730\text{ cm}^{-1} \quad (3)$$

where $\nu_{f,\text{NH}}$ is the frequency of the free N–H groups not participated in hydrogen bonding, $\nu_{b,\text{NH}}$ stands for the frequency of hydrogen bonded N–H groups, $\nu_{f,\text{CO}}$ is the frequency of free C=O groups, and $\nu_{b,\text{CO}}$ is the frequency of hydrogen-bonded C=O groups.

According to Table 2, $\Delta\nu$ is not zero for all the samples indicating that the N–H groups are involved in hydrogen bonding. Moreover, frequency shifts ($\Delta\nu$) for both the N–H and C=O stretching modes, and accordingly, the strength of hydrogen bonding for the studied samples are in the following order: PUCNT-2 > PU-1.7 > PU-2 > PUCNT-1.7 > PU-1. Since the strength of hydrogen bonding can be correlated with crosslinking density, mechanical and dynamic mechanical properties of the samples, these properties were investigated in the following.

Determination of Crosslink Density by Swelling Measurement

In the previous work [12], we reported a full investigation on the swelling behavior of the chemically cross-linked samples in a wide variety of non-polar to polar solvents. It should be reminded that PU-1, PUCNT-1.7 and PUCNT-2 are polymers with thermoplastic behavior, and therefore, only PU-1.7 and PU-2 (thermoset polymers) can be used for the swelling test. The inability to form the allophanate networks in PU-1 as a result of NCO/OH equal to unity, and also, the impediment effect of CNTs in PUCNT-1.7 and PUCNT-2

Table 2 The frequency shifts (chemical shifts) of the N–H and C=O stretching modes determined from FTIR spectra as a function of the NCO/OH molar ratio and adding of the CNT

Sample	$\Delta\nu_{\text{NH}}$	$\Delta\nu_{\text{CO}}$
PU-1	98	7
PU-1.7	130	24
PU-2	115	15
PUCNT-1.7	106	10
PUCNT-2	140	29

samples on cross-link formation are the main reasons for the obtained thermoplastic character.

To compare the CLD data obtained from swelling method with other methods (Young modulus, Mooney–Rivlin plots, G_R and DMA), CLDs were determined for PU-1.7 and PU-2 through swelling measurements in toluene, $\nu_{sw(in\ toluene)}$, and DMAc, $\nu_{sw(in\ DMAc)}$, and results were reported in Table 3. As is observed, the PU-2 (NCO/OH = 2) displays lower cross-link density than the PU-1.7 (with NCO/OH = 1.7) in the course of swelling for both of the solvents.

This unexpected behavior can be explained by the lower chain length of the PU-2 compared to PU-1.7 leading to a weaker phase separation during the post-curing process. Indeed, polyurethane phase separation is strongly sensitive to the soft segment molecular weight, the formation of hydrogen bonds between urethane linkages, the manufacturing process, soft segment type, and reaction. Herein, the molecular weight of chains and also formation of the hydrogen bonds between the urethane linkages can be considered as the major influential factors since others remained unchanged in samples. In general, the reaction between diisocyanate and polyester diol for the synthesis of polyurethane can be regarded as a step polymerization reaction, and thus, a reduction in molecular weight of the polyurethane chains can be occurred upon increasing the NCO/OH molar ratio. As the polyurethane molecular weight is stepped down, the phase mixing increases. Moreover, the molecular weight of the chains is an overriding factor since the higher molecular weights easily form rich phases on the entropic contribution. Here, it should be mentioned that in order to complete the crosslinking reactions, the pre-polymers were post-cured in the mold at a high temperature of 80 °C. Chains with higher molecular weight in PU-1.7 lead to a

higher level of inter-hydrogen bonding and phase separation; and therefore, result in more chemical crosslinking reactions compared to PU-2 during the post-curing process.

Swelling studies in toluene and DMAc revealed that the CLD is higher for the samples in toluene solvent rather than DMAc solvent. This observation can be related to various parameters such as solvent density, molar volume of solvent, the polymer–solvent interaction parameter (χ) [12], and also, different effects of these solvents on the chemical and physical networks which will be discussed later.

Tensile Behavior

The typical stress–strain curves for the sample films are illustrated in Fig. 4. In particular, the attention has been focused on some tensile parameters at low tensile strains (elastic deformation region) as Young’s modulus (E), modulus of resilience (E_R), offset yield stress (σ_Y), offset yield strain (ϵ_Y), and also, at high tensile strains (plastic deformation region) as modulus of toughness (E_T), strength and elongation at break (σ_B, ϵ_y) all of which are listed in Table 4. In order to perform a better comparison, the data reported in Table 4 were also shown in Fig. 5.

In the case of Young’s modulus, evaluated by dividing the tensile stress using the extensional strain in the elastic portion of the stress–strain curve, an exact same trend to the strength of the hydrogen bonding is also observed in the following order: PUCNT-2 > PU-1.7 > PU-2 > PUCNT-1.7 > PU-1 (Fig. 6; Table 2). This trend can be explained by some parameters such as hard segment concentration (NCO/OH molar ratio), crosslinking density, the effects of adding CNT, and also, strength of the hydrogen bonding between

Table 3 Comparison of network-related parameters applying tensile (Young’s modulus, Mooney–Rivlin and G_R methods), DMA and swelling tests to the studied samples

Sample	Tensile test methods								DMA method			Swelling method				
	Young’s modulus method			Mooney–Rivlin method			G_R method		T at min.	tan δ	E' at min.	tan δ	ν_{DMA}	ν_{tot}	ν_{ch}	ν_{ph}
	ρ	E	ν_E	$2C_1$	$2C_2$	ν_{MR}	G_R	ν_{GR}								
PU-1	1.18	30.3	4.08	7.384	0.82	3.31	1.49	0.6	326		9.33		0.57	–	–	–
PU-1.7	1.18	60	8.07	19	0.08	7.7	3.49	1.4	341		69.3		4.07	3.37	0.796	2.574
PU-2	1.19	51	6.86	13.04	1.65	5.93	4.26	1.72	338		54.04		3.21	2.43	0.674	1.756
PUCNT-1.7	1.22	37	4.98	13.21	–2.8	4.2	2.6	1.05	335		34.16		2.3	–	–	–
PUCNT-2	1.23	81.83	11	17.92	–1.2	6.75	2.93	1.18	343		45.41		2.65	–	–	–

The reported data for crosslink densities (ν) obtained from different methods are according to, mol cm^{-3} , and ($\times 10^{-3}$)

The reported data for Young’s modulus (E), constant parameters of Mooney–Rivlin curves ($2C_1$ and $2C_2$), strain hardening modulus (G_R) and storage modulus at minimum tan δ –T curve (E') are according to MPa

The reported data for samples density (ρ) and temperature at minimum tan δ –T curve (T) are according to g cm^{-3} and kelvin, respectively

$$\nu_{tot} = \nu_{sw\ (in\ toluene)} \text{ and } \nu_{ch} = \nu_{sw\ (in\ DMAc)}$$

$$\nu_{ph} = \nu_{tot} - \nu_{ch}$$

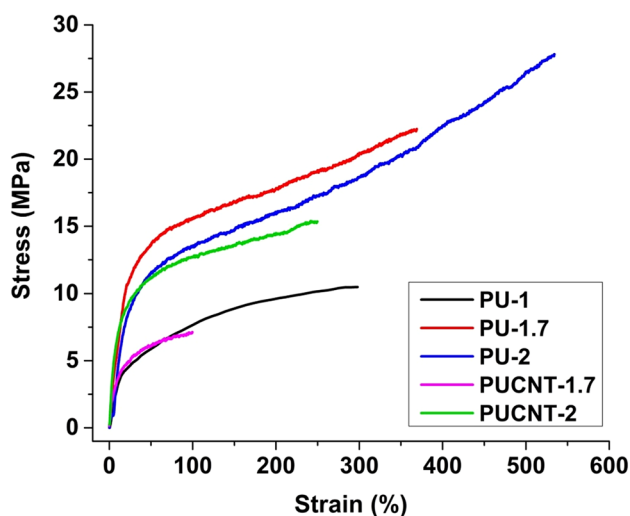


Fig. 4 Representative stress–strain curves for PUs and PU/CNTs nanocomposites

PU segments or CNTs with PU hard segments as observed from FTIR analysis results.

The effect of CNT introduction on the elastic modulus in the tensile test could be evaluated by its corresponding nanocomposite sample containing 0.5 wt% CNT. Here, CNT can be effective on the elastic modulus through two opposing effects. First, the steric hindrance effect of CNTs can be the reason for reduction of the reactions between $-NCO$ groups and $-OH$ groups of the as-synthesized polyurethane nanocomposites, and thereby, formation of urethane groups and hard segments is diminished. Since modulus is higher for hard segment than soft segment, the steric hindrance effect of CNTs caused the elastic modulus to decrease. Second, the reinforcing effect of CNTs that is due to interactions between CNTs' functional groups and PU's urethane groups ($-HNC=O$), and also, high modulus of the CNTs themselves. As is seen in Fig. 5, the dominant role of the CNTs' steric hindrance in PUCNT-1.7 caused a notable decline in Young's modulus as compared with the other samples. On the other hand, in the nanocomposite samples, with increasing of NCO/OH molar ratio from 1.7 to 2, more isocyanate

moles remain unreacted which have the potential for reacting with hydroxyl groups of both Polyol and CNTs. Therefore, for PUCNT-2, the reinforcing effect of CNTs is preferred over the steric hindrance effect leading to higher modulus for this sample as compared with other samples.

Since the NCO/OH molar ratio in polyurethane synthesis has a direct influence on the hard segment concentration, strength of hydrogen bonding and finally elastic modulus, the lowest value of Young's modulus was observed for PU-1 which could be attributed to the lower hard segment content in this sample. Nevertheless, further increment of NCO/OH molar ratio from 1.7 to 2 for PU-1.7 and PU-2 caused a decrease in the modulus. This unexpected result could be ascribed to the higher crosslink density of PU-1.7 as compared to PU-2 which was found based on the swelling results.

The resilience's modulus is defined as the maximum energy that can be absorbed per unit volume without creating a permanent distortion. It was calculated by integrating

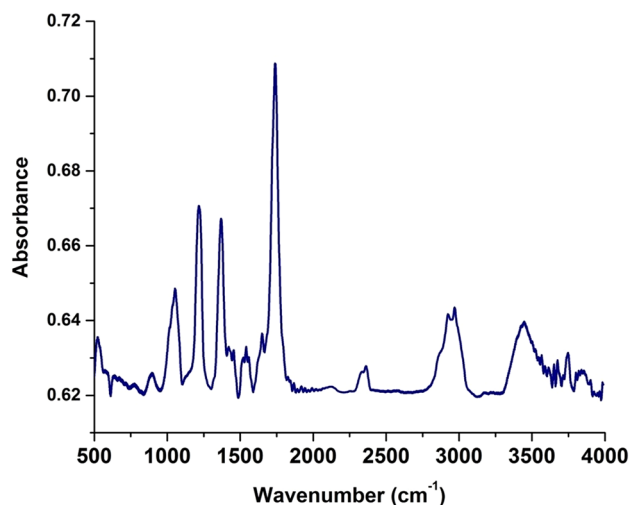


Fig. 5 Comparison of tensile properties of PUs and PU/CNT nanocomposites: **a** Young's modulus, **b** resilience's modulus, **c** 0.2% offset yield stress, **d** toughness' modulus, **e** tensile strength, and **f** elongation at break

Table 4 Mechanical properties of the PUs and PU/CNT nanocomposites

Sample	Young's modulus (MPa) (E)	Resilience's modulus (E_R) (MPa)	0.2 % offset yield stress (σ_Y) (MPa)	0.2 % offset yield strain (ϵ_Y) (MPa)	Tensile strength (σ_B) (MPa)	Strain at break (ϵ_B) (%)	Toughness' modulus (E_T) (MPa)	Shore A hardness	Weight loss by abrasion (%)
PU-1	30.3	0.218	4	10.2	10.5	300	24.23	81	13.8
PU-1.7	60	0.94	10.7	18.313	22.25	370	62.7	92	5.8
PU-2	51	0.66	8.5	16.3	28	534	96.5	90	7.2
PUCNT-1.7	37	0.2	3.7	3.8	7.13	100	5.64	84	22.9
PUCNT-2	81.8	0.23	7.4	7.9	15.4	250	31.2	95	10.5

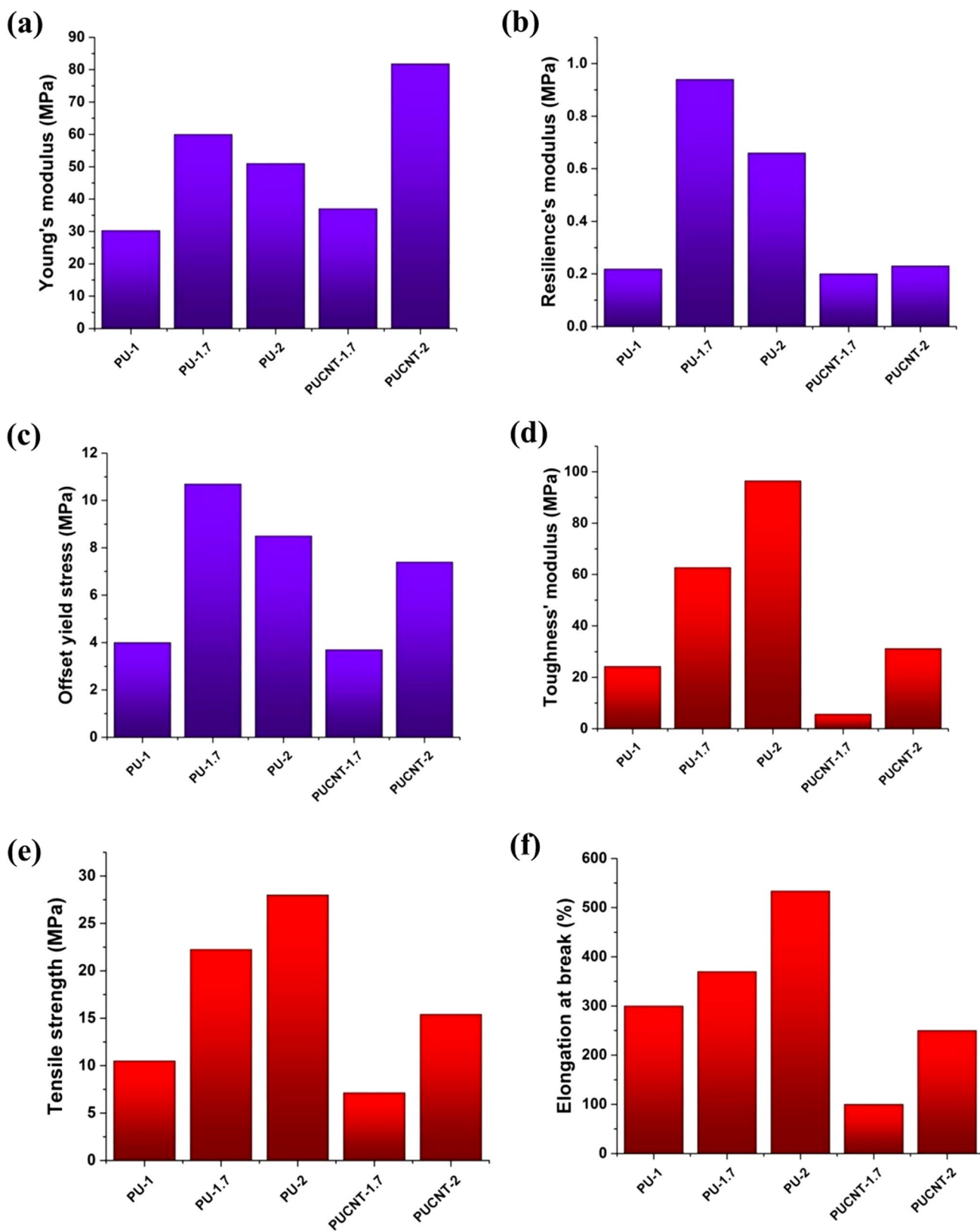


Fig. 6 Absorbance FTIR spectroscopy of PUs and PU/CNT nanocomposites in ATR mode

the stress–strain curve from zero to the elastic limit, and the attained data were tabulated in Table 4. As is clear from Table 4 and Fig. 5, the resilience modulus of PU-1.7 and PU-2 were notably decreased upon introduction of CNT. Such behavior can be attributed to the existence of chemical crosslinks in PU-1.7 and PU-2 which increased the linear region (elastic deformation region) for PUs in comparison to their corresponding nanocomposites. However, the resilience's modulus of the PUs and also nanocomposites conform the following order: PU-1.7 > PU-2 > PU-1 and PU-CNT-2 > PU-CNT-1.7. Similar to the elastic modulus, such trend for resilience modulus can also be ascribed to the crosslink density, NCO/OH molar ratio and the opposed effects of CNT.

Another concept at linear region of stress–strain curve, which is widely used in engineering applications, is yield stress. Several different definitions of the yield point have been used to assess the yield stress. Many researchers considered the upmost of the stress–strain curve as the yield stress. The offset stress is also used, especially when the stress–strain curve reveals no clear maximum. In this study, offset yield points (including offset yield stress and strain) were determined for samples and the obtained data were reported in Table 4. Figure 7 also illustrates how to obtain the offset yield point. It has been given by the intersection of the stress–strain curve with a straight line that has the same initial slope as the stress–strain curve but is offset on the strain axis by a determined strain, e.g., 0.2%. Since offset yield stress is directly related to resilience, similar trends are observable for offset yield data of the samples in Fig. 5c.

As is clear from Fig. 5, different trends can be observed for samples in high tensile strain in comparison to low

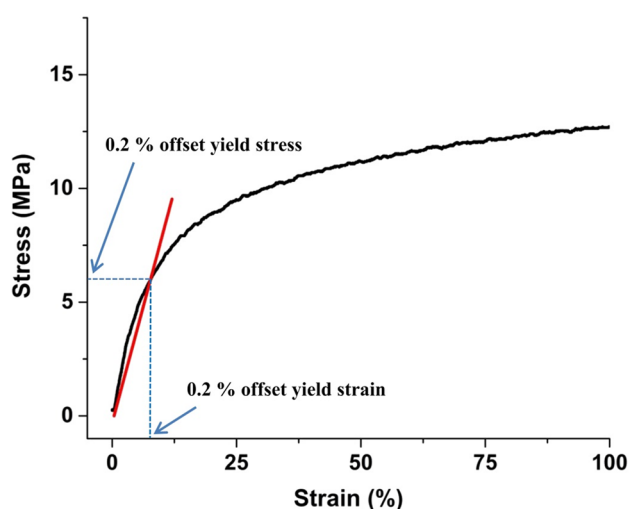


Fig. 7 Part of the stress–strain curve of PUCNT-2 sample (black line). The 0.2% offset yield stress and strain were indicated by the intersection with the straight red line

tensile strain. The toughness, tensile strength and elongation at break of the PUs were higher than those of the corresponding nanocomposites. For instance, the toughness' modulus of PUs containing NCO/OH molar ratios of 1.7 and 2 were increased by 11.1 and 3.1 times, respectively, as compared to their corresponding nanocomposites. In this case, 0.5 wt% CNT loading caused to the change of character from the thermoset into thermoplastic. In fact, formation of crosslinks was impeded due to the steric hindrance effect of CNTs which might be the reason for the reduced abovementioned parameters in high tensile strains.

The results indicate that the dominant role of the reinforcing effect of CNTs in NCO/OH molar ratio of 2 is more pronounced than that of 1.7. Therefore, CNT in PUCNT-2 sample improved the toughness' modulus, tensile strength and elongation by about 5.5, 2.16 and 2.5 times, respectively, as compared with PUCNT-1.7.

Moreover, a comparison between PUs reveals that the toughness, tensile strength and elongation were enhanced as NCO/OH molar ratio increased (Fig. 5d–f). This could be interesting since the Young's modulus, the resilience modulus and the offset yield stress, that are related to the elastic deformation region, are higher for PU-1.7 than PU-2, but the toughness, tensile strength and elongation at break, that are related to the plastic deformation region, were enhanced for PU-2 in comparison to PU-1.7. As it became clear from the swelling experiments, the crosslink density and also chain stiffness for PU-1.7 are higher than PU-2. Such result explains the enhanced Young's modulus, resilience and offset yield stress in the low tensile strain (elastic deformation portion) for PU-1.7. On the other hand, in the high tensile strain, the increased chain mobility in PU-2 leads to a better phase separation, and thus, strain hardening. This consideration would explain the higher value of Young's modulus, resilience and offset yield stress in high tensile strain for PU-2 compared to PU-1.7.

Determination of Crosslink Density by Stress–Strain Measurement

Stress–strain measurements are one of the most efficient and powerful methods for the calculation of CLDs which have great advantages since they need no complex equipment for standard testing methods, and also due to the fact that samples can be examined directly in the desired state without any extra preparations such as swelling or similar procedures [20]. Moreover, unlike stress–strain measurement methods, the physical crosslinking density determination using swelling method cannot be carried out for the thermoplastic samples.

The most important methodologies to determine CLD, based on stress–strain characteristics, are the Young modulus method (E), the Mooney–Rivlin method (MR) and the

strain hardening modulus (G_R), which have been obtained from the phenomenological theory of rubber elasticity. In the following, CLD determination by using each of these methods will be described for the PU-1, PU-1.7, PU-2, PUCNT-1.7 and PUCNT-2.

The initial slope can be considered to be Young's modulus (E). Therefore, E values for the polyurethanes and nanocomposites were determined from the initial slope of the stress–strain curves. Based on the theory of rubber elasticity, E is related to the CLD by the Eq. (4).

$$E = 3\nu_E RT \quad (4)$$

where ν_E is the obtained crosslinking density from Young modulus method, R is universal gas constant ($8.314 \text{ J mol}^{-1} \text{ K}^{-1}$) and T is the absolute temperature (K). The ν_E data for the studied samples are shown in Table 3. According to that table, the crosslinking density trend, obtained via Young modulus method, is in the following order: PUCNT-2 > PU-1.7 > PU-2 > PUCNT-1.7 > PU-1 which is similar to the Young modulus trend as previously discussed.

Another method for determination of CLD from stress–strain plots is Mooney–Rivlin method. The Mooney–Rivlin equation has been widely used for the determination of the degree of crosslinking for a wide variety of polymers. The equation is based on the phenomenological theory of rubber elasticity, which is shown by Eq. (5).

$$\sigma / (\lambda - \lambda^{-2}) = C_1 + C_2 \lambda^{-1} \quad (5)$$

In the above equation, σ is the uniaxial tensile stress, λ is the extension ratio evaluated as the ratio of the deformed length to the original length when the specimen is dragged uniaxially, and C_1 and C_2 are characteristic constants of the sample.

In Fig. 8, the expression on the left-hand side of Eq. (5) is plotted versus λ^{-1} for the PU-1, PU-1.7, PU-2, PUCNT-1.7 and PUCNT-2 samples. Obviously, one obtains a series of curves where the intercept and the slope of the curves attributed to the value of $2C_1$ and $2C_2$, respectively. Experimental data on $2C_1$, $2C_2$ are shown in Table 3. It has been indicated that the physically effective crosslink density can be calculated from the parameter C_1 . The parameter C_2 has been related to the intermolecular forces, e.g. entanglements. The upturn at a relatively higher elongation is owing to the strain-induced crystallization and also high extensibility of the chains. At low strains, both $1/\lambda$ and $(\lambda - \lambda^{-1})$ are sensitive to the experimental error in the extension ratio measurements. Therefore, herein, the data were taken in the range between $\lambda^{-1} = 0.9$ and $\lambda^{-1} = 0.2$. The observed decline in $\sigma/2(\lambda - 1/\lambda^2)$ at low stretch ratios can be due to Payne effect. The Mooney–Rivlin crosslink density (ν_{MR}) of polyurethanes and nanocomposites

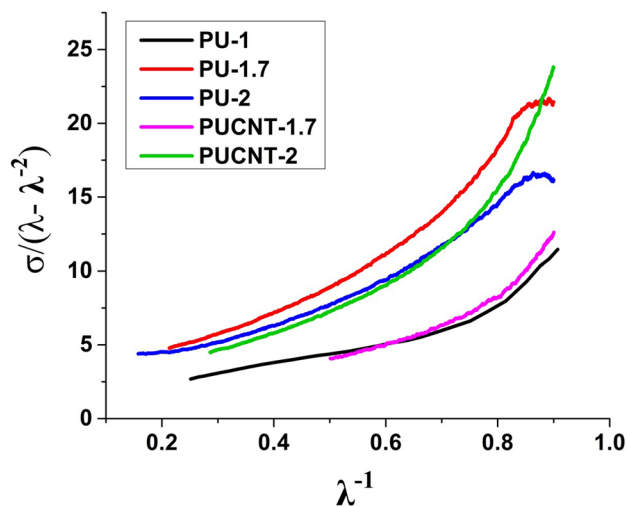


Fig. 8 Mooney–Rivlin graphs obtained for PUs and PU/CNTs nanocomposites

were determined from the constant C_1 with the following expression and the results are shown in Table 3.

$$\nu_{MR} = C_1 / RT \quad (6)$$

where R is the universal gas constant and T is the temperature in Kelvin scale at which the stress–strain measurements are made.

The strain hardening modulus (G_R) at 90% of the ultimate true strain can also be used for calculating of CLD. The true stress (σ_T) versus neo-Hookean strain ($\lambda^2 - 1/\lambda$) curves of samples are displayed in Fig. 9. Here, G_R is the slope of the true stress (σ_T) versus $(\lambda^2 - 1/\lambda)$ as shown by Eq. (7).

$$G_R = \frac{-\partial \sigma_T}{\partial (\lambda^2 - 1/\lambda)} \quad (7)$$

The crosslink density of the polyurethane samples (ν_{GR}) can be calculated by the following equation:

$$\nu_{GR} = G_R / RT \quad (8)$$

where R is the ideal gas constant and T is the absolute temperature (K). The values of G_R and ν_{GR} of all the polyurethanes and nanocomposites are tabulated in Table 3 which show the following trend: PU-2 > PU-1.7 > PUCNT-2 > PUCNT-1.7 > PU-1.

Since the obtained CLD from G_R method is based on the polymer response at high strains, the difference between ν_{GR} of samples in this method can be related to the chemical crosslinking, phase separation, strain hardening capability and hard segment content.

The presence of chemical crosslinks in the PU-2 and PU-1.7 samples caused higher ν_{GR} for these two samples in comparison to others. Moreover, the enhance level of

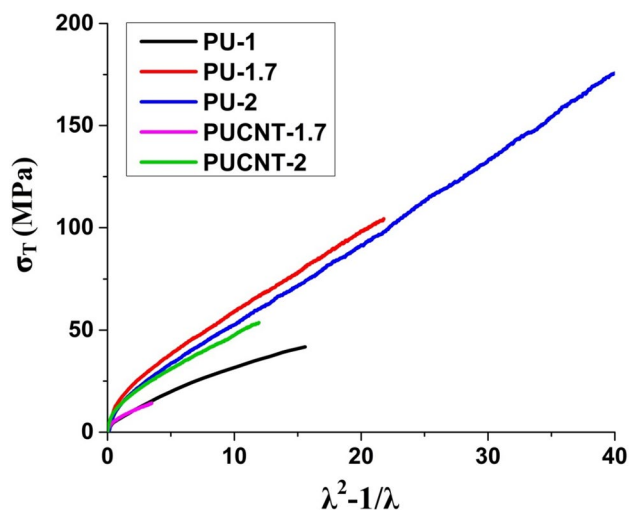


Fig. 9 True stress (σ_T) versus neo-Hookean strain ($\lambda^2 - 1/\lambda$) curves for the PUs and PU/CNTs nanocomposites

phase separation for PU-2 at high strains leads to higher strain hardening, and finally, increase the ν_{GR} of this sample compared to PU-1.7. In the nanocomposite samples, for PUCNT-2, the reinforcing effect of CNT is preferred over the steric hindrance effect, and caused an increase in ν_{GR} for this sample as compared with PUCNT-1.7 sample. The lowest observed values of ν_{GR} for PU-1 could be attributed to the weak interaction between polymer chains at high strains because of the lower hard segment content in this sample.

Dynamic Mechanical Thermal Analysis (DMTA)

DMTA is the most useful technique for studying the viscoelastic behavior of polymers wherein results are expressed by three main parameters: the storage modulus (E'), which is the elastic response to the deformation; the loss modulus (E'') representing the viscous portion of a viscoelastic material under deformation, that is useful for detecting the occurrence of molecular transitions such as the glass transition temperature ($T_{g,E''}$); and damping behavior ($\tan \delta$) which can be obtained from the ratio of E'' to E' , sometimes temperature at which $\tan \delta$ peaks is taken as the glass transition temperature ($T_{g,\tan \delta}$). DMTA analysis was carried out to evaluate the temperature dependence of E' , E'' , and $\tan \delta$ of the polyurethanes and corresponding nanocomposites, which are depicted in Fig. 10. As is expected, E' decreases with increasing temperature for all samples, which can be ascribed to the increased molecular mobility of the polymer chains [21]. Moreover, all samples displayed a relaxation process, which is related to the glass–rubber transition. It is clear that as the temperature rises, the loss modulus and damping values pass through a maximum in the transition region, and then, decrease in the rubbery region.

This relaxation process includes the release of cooperative motions of chains in the segments and between crosslinks. Below T_g , the loss modulus and damping are low since, in this region, the chain segments are in the frozen state. Accordingly, the deformations are primarily elastic and the molecular slips, resulting in the viscous flow, are insignificant. In the rubbery region, the molecular segments are entirely free to move (especially for the thermoplastic samples) whereby the loss modulus and damping are low [22]. Nevertheless, in the transition, the molecular chains and also frozen segments begin to move, and their excess energy is released as heat. In fact, a frozen segment in the glassy state can store more energy for a given deformation than a rubbery segment that can freely move. In a region, where most of the chain segments participate in a cooperative motion under a given deformation, the maximum loss modulus or damping would occur [23, 24].

Moreover, as seen in Fig. 10 and Table 5, the dynamic storage modulus, temperatures at loss modulus peak ($T_{g,E''}$) and also $\tan \delta$ peak ($T_{g,\tan \delta}$) conformed the following trend: PUCNT-2 > PU-1.7 > PU-2 > PUCNT-1.7 > PU-1. Since such trend is exactly similar to the trends observed with respect to the Young's modulus in tensile test and chemical shifts in FTIR spectra for the studied samples, one could infer that DMTA results further confirm the tensile and also FTIR results as well. As previously described, the dominant role of the reinforcing effect of CNTs in PUCNT-2 caused to maximum storage modulus at temperatures from -100 to 100 °C ($E'-T$ curves), $T_{g,E''}$ and also $T_{g,\tan \delta}$. This can be attributed to the low value of adhesion factor (A) and thus low segmental motions of polymer at the CNT surface (Polymer-CNT interface) which will be discussed later.

The presence of the chemical crosslinks in PU-1.7 and PU-2 led to improve E' , $T_{g,E''}$ and $T_{g,\tan \delta}$ for these samples as compared to PUCNT-1.7 and PU-1. It should be noted that crosslink density and thus E' , $T_{g,E''}$ and $T_{g,\tan \delta}$ for PU-1.7 were higher than PU-2. The dominant role of the steric hindrance of CNTs in PUCNT-1.7 caused E' and T_g to decrease as compared with PUCNT-2, PU-2 and PU-1.7. Finally, the lowest NCO/OH molar ratio and thermoplastic behavior in PU-1 led to observation of the minimum E' and T_g for this sample.

In addition to the temperature at $\tan \delta$ peak, peak height and peak width at half height (FWHM) are indicative of the structure and properties of materials. These parameters were obtained and summarized in Table 5.

The width of the $\tan \delta$ peak can be related to the system heterogeneity [25]. As the NCO/OH molar ratio of the polyurethanes increased, FWHM showed an ascending trend (23.77, 34.32 and 43.85 for PU-1, PU-1.7 and PU-2, respectively). Distribution of hard segments length and energy dissipation among hard segments leads to this phenomenon especially when networks are under strain [26].

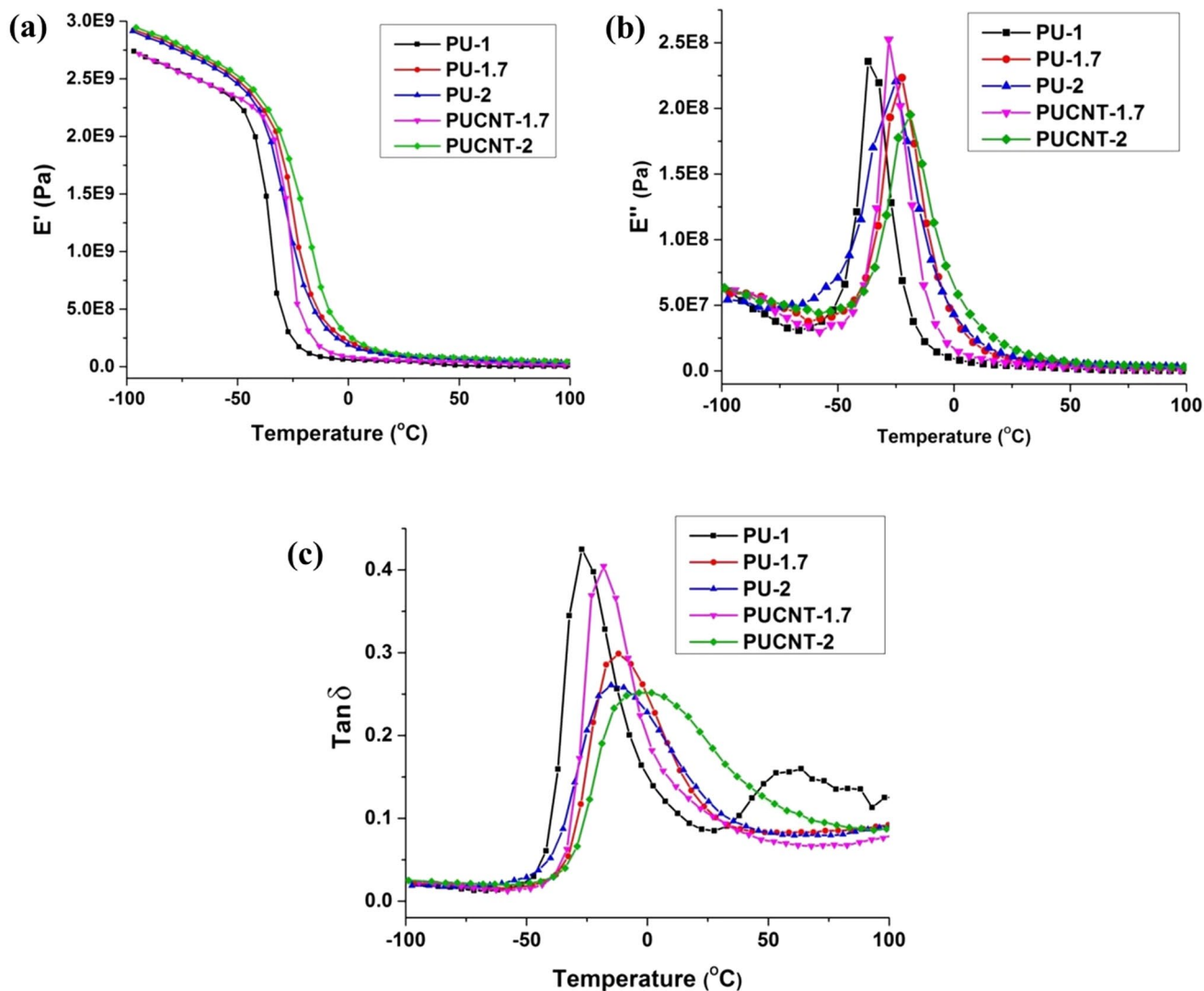


Fig. 10 Results of dynamic mechanical analysis of **a** storage modulus, **b** loss modulus, and **c** damping factor ($\tan \delta$) of PUs and PU/CNTs nanocomposites

Table 5 The obtained parameters from DMTA curves of the PUs and PU/CNT nanocomposites

Sample	Glass transition temperature (°C)		Tan δ peak width at half height (FWHM)	Tan δ peak height	Adhesion factor (A)
	From E'' vs. T curve	From tan δ vs. T curve			
PU-1	-36.9	-26.8	23.77	0.424	-
PU-1.7	-22.2	-11.9	34.32	0.3	-
PU-2	-25.5	-14.5	43.85	0.26	-
PUCNT-1.7	-28	-17.6	24.3	0.4	0.333
PUCNT-2	-18.8	-0.75	55.7	0.25	-0.0384

Moreover, the wider peak of $\tan \delta$ obtained for PU-2 indicates a less homogeneous distribution of crosslinks than PU-1.7 as it became clear from the swelling tests. Another interesting observation is related to the maximum FWHM

for PUCNT-2 in comparison to the minimum FWHM for PUCNT-1.7. This phenomenon might be due to the higher CNT aggregations in PUCNT-2 compared to PUCNT-1.7 (see SEM).

In the following, the $\tan \delta$ peak height and adhesion factor (A) were used for evaluation of the chain mobility and interfacial adhesion (Table 5). Since a lower peak height indicates a less chain mobility and good interfacial adhesion, lower values of the peak height for PU-1.7 and PU-2, as compared with PU-1, were attributed to the inter-chain chemical bonds (chemical crosslinks) and thereby reduction of the chain mobility in these two samples.

In order to confirm the opposing effects of the CNT particles in PUCNT-1.7 and PUCNT-2 by $\tan \delta$ -T curves, the adhesion factor (A) values were evaluated. Kubař explained that the effect of the interphase region on the dynamic properties can be quantified in a direct way. The mechanical loss factor, $\tan \delta_c$, of the composite can be assumed and expressed as Eq. (9).

$$\tan \delta_c = \Phi_f \tan \delta_f + \Phi_i \tan \delta_i + \Phi_p \tan \delta_p \quad (9)$$

where the subscripts f, i, and p stand for the filler, interphase, and polymer matrix, respectively, and Φ is the corresponding volume fraction. Obviously, Eq. (9) cannot provide a detailed prediction of the mechanical loss factor of the composites since it includes a combination of parallel and series coupling of the phases.

Nevertheless, it can be used to compare the effect of different surface treatments on the state of adhesion between the phases. By assuming that the volume fraction of the interphase is very small and that $\tan \delta_i \cong 0$, Eq. (9) can be rearranged to:

$$\frac{\tan \delta_c}{\tan \delta_p} \cong (1 - \Phi_f)(1 + A) \quad (10)$$

$$A = \left[\frac{\Phi_i}{1 - \Phi_f} \right] \left(\frac{\tan \delta_i}{\tan \delta_p} \right) \quad (11)$$

In the nanocomposites, strong interactions between the filler (CNT) and the polymeric matrix at the interface tend to reduce the polymer chains mobility in the adjacency of the nanoparticle surface compared to that in the bulk matrix, which reduces $\tan \delta_i$ and thus A . A low value of A demonstrates a low molecular mobility surrounding the nanoparticles and a high degree of interaction between CNTs and polyurethane chains.

However, Table 5 shows a decrease in A value for PUCNT-2 ($A = -0.038$) compared with PUCNT-1.7 ($A = 0.333$). Therefore, this result confirms a strong interaction between CNT and hard segment in PUCNT-2 (the reinforcing effect of CNT particles), and in opposite, a weak interaction between them in PUCNT-1.7 (the steric hindrance effect).

The homogeneity of the samples can be studied by using cole–cole plots. Homogeneous polymeric systems are

reported to show semi-circle diagram since two-phase systems show two modified semi-circles [27]. The cole–cole plots of the polyurethanes and nanocomposites are provided in Fig. 11, and are imperfect semi-circles indicating heterogeneity of the system. However, the reasons for this behavior can be the presence of both hard and soft segments (in all samples), chemical crosslinks (in PU-1.7 and PU-2) and CNT particles (in PUCNT-1.7 and PUCNT-2).

Determination of Crosslinking Density by DMTA Measurement

CLD of the synthesized PUs and PU/CNTs can also be evaluated from experimentally measured rubbery plateau E' values through the following equation:

$$\nu_{\text{DMA}} = E_r/6RT \quad (12)$$

However, the rubber plateau for thermosets is not as distinguished as for thermoplastics. The rubber plateau modulus (E_r) is described in this region, as the ‘most elastic’ dynamic modulus found at the lowest value of $\tan \delta$ [28–30]. Quite expectedly, E_r values and the resulting ν_{DMA} values (see Table 3) are the maximum values for thermoset samples (PU-1.7 and PU-2) and the minimum for PU-1. For PU/CNT nanocomposites, it should be considered that the existence of high amount of diisocyanate during in situ polymerization caused a weaker hindrance effect of CNT particles for PUCNT-2 in contrary to PUCNT-1.7. Therefore, hydroxyl functional groups on the surface of CNTs in PUCNT-2 can establish good interactions with -NCO groups, and also, hard segments in PU chains. These interactions are responsible for the higher E_r and ν_{DMA} values for PUCNT-2 compared with PUCNT-1.7. Nevertheless, since these interactions are more of physical type, which caused thermoplastic behavior,

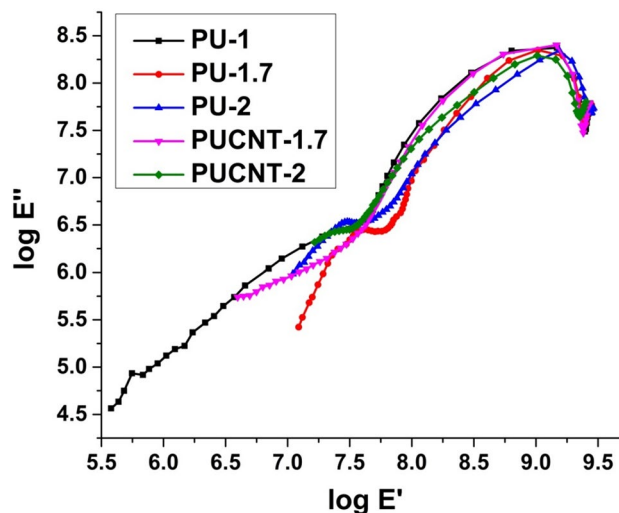


Fig. 11 Cole–Cole plots of the PUs and PU/CNT nanocomposites

lower E_r and ν_{DMA} values for PUCNT-2 as compared with thermoset samples (PU-1.7 and PU-2) were justified. Lastly, as previously mentioned higher chains' molecular weight in the case of PU-1.7 caused a higher level of inter-hydrogen bonding, phase separation and also chemical crosslinks rather than PU-2 resulting in the maximum E_r and ν_{DMA} values for PU-1.7.

Comparison of CLD Values Obtained from Various Methods

Several methods have been reported for measuring CLD including swelling and methodologies that are based on stress–strain, DMTA, small-angle neutron scattering, atomic force microscopy, NMR, freezing-point depression and gas chromatographic. However, the swelling, stress–strain (Young's modulus, Mooney–Rivlin and G_R) and also DMTA methods continue to be popular due to their simplicity. Therefore; in the present work, we used those three methods to study CLD of the synthesized samples which are based on the basic rubber elasticity theory.

It should be noted that the experimentally determined CLDs include both chemical crosslinks due to excess of NCO/OH molar ratio in the system and formation of the allophanate linkages, and also, physical crosslinks which originate from the chain entanglements. The physical crosslinks are comprised of two categories: (1) permanently chain entanglements and (2) temporarily (sliding) chain entanglements.

At small extensions of the tensile test, the contribution to the modulus by temporarily physical entanglements is quite significant; however, such contribution is decreased with increase of the strain. At larger extensions, the chemical and permanent physical crosslinks outweigh the temporary physical entanglements in determining the modulus. Hence, ν_E is the sum of contributions from all three types of crosslinks; while ν_{MR} can be a combination of chemical crosslinks and permanent physical entanglements. At very large extensions (90% of the ultimate true strain), the CLD (ν_{GR}) can be expected to be only comprised of the chemical crosslinks and a small part of the permanently physical crosslinks. Therefore, trends observed for CLD values determined via tensile test method can be justified according to order: $\nu_E > \nu_{MR} > \nu_{GR}$ (Table 3). As is clear from Table 3, the CLDs determined by DMTA technique (ν_{DMA}) exhibit lower values compared to ν_E and ν_{MR} which may be related to the high temperatures (about 100 °C) in rubbery plateau region that caused a reduction in chemical and physical crosslink values, and thus ν_{DMA} .

CLDs determined through swelling measurements (ν_{sw}) are under diffusion control contrary to other CLDs (ν_E , ν_{MR} , ν_{GR} and ν_{DMA}) which are generally under modulus control. Since diffusion phenomena were performed with slow rates

compared with stress–strain and storage modulus responses, the swelling crosslink density values (ν_{sw}) for the chemical cross-linked samples (PU-1.7 and PU-2) were less than ν_E , ν_{MR} and ν_{DMA} .

Although it is impossible to individually determine the chemical and physical crosslinks through tensile and DMTA techniques, swelling measurements allows one to determine them separately. To this end, toluene (for soft segments) and DMAc (for hard segments) were used as appropriate solvents. It was observed that samples in DMAc absorbed the solvent and swelled very well as compared to the toluene solvent, which can be explained by the polymer–solvent interaction parameter (χ) [12], and also different effects of those solvents on the chemical and physical crosslinks. For a poor solvent, such as toluene, the swelling is governed by both physical (ν_{ph}) and chemical (ν_{ch}) cross-linking. Hence, a total CLD, ν_{tot} , can be determined. On the other hand, DMAc, as a good solvent, destroys the domain structure of the polyurethanes so that only the effects of chemical cross-linking may be detected (ν_{ch}). Accordingly, the following equations can be presented:

$$\nu_{sw}(\text{in toluene}) = \nu_{tot} = \nu_{ch} + \nu_{ph} \quad (13)$$

$$\nu_{sw}(\text{in DMAc}) = \nu_{ch} \quad (14)$$

$$\nu_{ph} = \nu_{sw}(\text{in toluene}) - \nu_{sw}(\text{in DMAc}) \quad (15)$$

The physical and chemical cross-linking data for PU-1.7 and PU-2 are shown in Table 3.

Hardness and Abrasion Measurement

As a general principle, Shore A hardness increases with increasing of the Young modulus, Tg, crosslink density and also adding of fillers. Therefore, the observed trend for the studied samples in Fig. 12a and Table 4 can be related to the abovementioned parameters which are conforming with the obtained previous results from FTIR spectra, Young modulus trends in tensile tests, swelling tests, the Tg trends which were determined using DMTA technique and also TGA results in our previous work [12, 31, 32]. In the following, these trends also will be further evaluated through SEM and AFM techniques.

As is seen in Fig. 12b and Table 4, the observed trends about percentage of abrasion weight loss, especially with comparison of PUs and their corresponding nanocomposites, are different than hardness trends. This can be attributed to the applied shear stress on the sample surface during abrasion test which leads to withdraw of nano-fillers from the PU matrix causing the creation of voids and cracks, and thus, the abrasion resistance is further reduced for the nanocomposite sample as compared with the corresponding polyurethane. Moreover, since increasing NCO/OH molar ratio resulted in

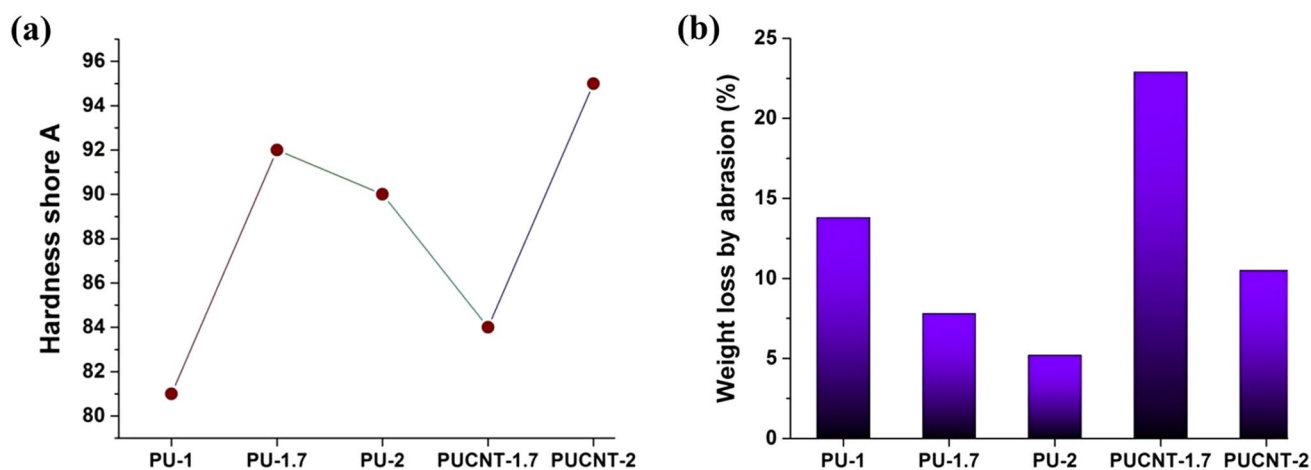


Fig. 12 Comparison **a** hardness (shore A) and **b** abrasion resistance of PUs and PU/CNTs nanocomposites

increasing of the chemical and physical interactions between polymer chains or CNT and polymer chains, the abrasion resistance improved for both PU-2 and PUCNT-2.

Morphological Observations

In order to investigate the influence of NCO/OH molar ratio and CNTs on the surface properties of PUs and PUCNT-2, AFM analysis in phase mode was performed. The AFM 2D images of the synthesized samples with corresponding histograms are shown in Figs. 13 and 14, respectively. In the AFM images, the brighter and darker regions represent the hard regions and the soft regions, respectively.

The AFM images and histograms reveal that surface hardness and the resulting surface modulus for PUs are in the order of: PU-1.7 > PU-2 > PU-1 which is in accordance with the hardness test, Young's modulus, DMTA and FTIR results. Also, the presence of CNTs in PUCNT-2 leads one to observe more heterogeneity and hard regions in the AFM images and histograms compared with those of other samples. This observation can be related to both high modulus and reinforcing effect of CNT nanoparticles which was previously discussed.

Figure 15 shows the SEM images of the nanocomposite samples PUCNT-1.7 (Fig. 15a) and PUCNT-2 (Fig. 15b). Comparing the morphology of PUCNT-1.7 and PUCNT-2, larger agglomerations are observed for the PUCNT-2 while the better dispersion of CNT nanoparticles in the matrix can be seen for the PUCNT-1.7. However, once the NCO/OH molar ratio is further increased from 1.7 to 2, the hindrance effect becomes weaker due to the very high amount of diisocyanate in the system, and thus, the reinforcing effect is dominated leading to the better adhesion between CNT-Polymer and also CNT-CNT nanoparticles (resulting agglomeration of CNT nanoparticles).

According to the previous analyses, the higher modulus, Tg and hardness obtained for PUCNT-2 as compared with other samples is due to the reinforcing effect of CNTs in this sample which is further confirmed through TEM images. As is clear from TEM images (Fig. 16), the interfacial area between the PU matrix and carbon nanotubes is utterly continuous (the interface cannot be evidently detected), which demonstrates a strong bonding between the PU matrix and carbon nanotubes via chemical bonds between isocyanate groups and -OH groups residing on the surface of CNTs, and also, through physical interactions between hard segments of the polyurethanes with -COOH groups on the surface of CNTs.

Remarks on the Effect of CNTs

In order to gain a deeper insight into the polymerization reaction in the presence of CNT nanoparticles and also their role in the observed thermoplastic character, an attempt was made to illustrate a schematic representation of the proposed mechanism in Fig. 17. As can be seen, in the case of PUCNT-1, the number of diisocyanates is equal to that of polyols. As the reaction commences, due to the hindrance effect of CNTs, diisocyanate molecules are not able to approach the polyol molecules, and as a result, only a few number of urethane groups will be formed. In fact, an equal number of diisocyanate and polyol molecules cannot lead to formation of polymer molecules due to the presence of CNT, and thus, one could infer that the number of diisocyanate molecules shall be increased in order to dominate the CNT's hindrance effect. One could infer that if CNT was eliminated from the reaction chamber in this sample, those diisocyanates which were not able to approach the polyols, will now be reacted easily with the free polyol groups resulting in formation of thermoplastic polyurethane (PU-1).

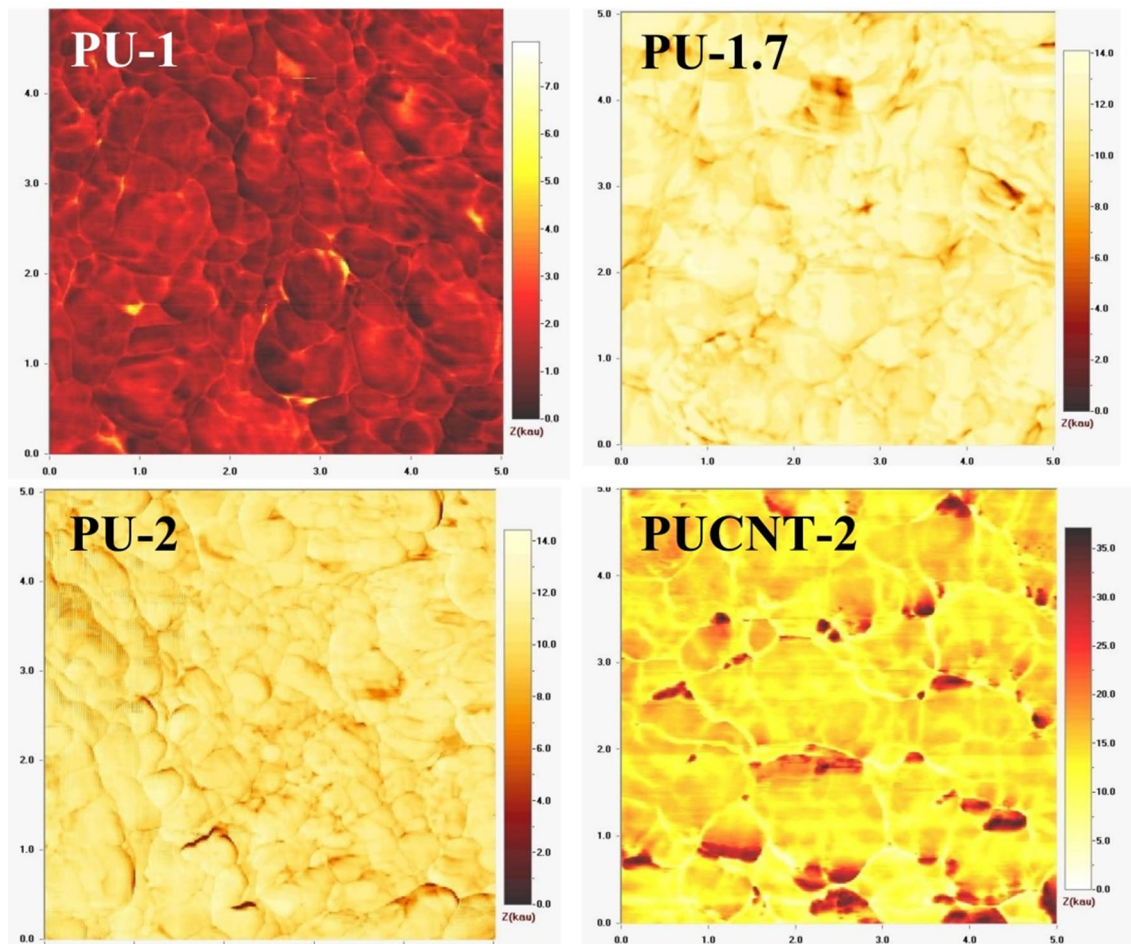


Fig. 13 AFM 2D images of PU-1, PU-1.7, PU-2 and PUCNT-2 nanocomposites

All in all, in the case of PUCNT-1, the CNT particles have exhibited no trace of their reinforcing effect but instead the steric hindrance effect was dominant leading to formation of a useless powder.

Based on the attained results, one could speculate that as the number of diisocyanates increases, the polymerization reaction would partly take place. As compared with the previous sample (PUCNT-1), the excess diisocyanate molecules can react with two types of polyols. The first group are those polyols which are localized in the vicinity of CNTs, and the second group are related to those polyols which are localized farther from the CNTs. Due to the hindrance effect of CNTs, the diisocyanate groups would rather react with the latter polyol group; however, since the number of excess diisocyanates is limited, they will be reacted, and eventually, no further diisocyanate groups would remain. Therefore, the hindrance effect of CNTs is still more dominant than its reinforcing effect in the case of PUCNT-1.7. It should be noted that a number of diisocyanate molecules might be bound/trapped around CNTs, and as a result, they cannot participate

in the polymerization reaction. If the CNT component is eliminated from this sample, those trapped diisocyanates would be allowed to participate in the reaction and even result in network formation via crosslinking the PU chains. As a result, the PU-1.7 sample with thermoset character will be formed.

As the number of diisocyanates is further increased, after reacting with the second type of polyols, there still exist excess diisocyanates which could react with the first type of polyols (closer to CNTs) leading to formation of much longer PU chains. Moreover, after reacting those polyols in the vicinity of CNTs, PU chains will be formed around the CNT particles which results in establishment of interactions between the urethane groups of the chain and hydroxyl groups residing on the CNTs' surfaces. Such interactions might lead to stronger connections among PU chains and CNTs reducing the mobility of polymer chains, which is responsible for the increased T_g , Young modulus, storage modulus, abrasion resistance, hardness and etc. as compared to the PUCNT-1.7. It is worthy to mention that the CNT's

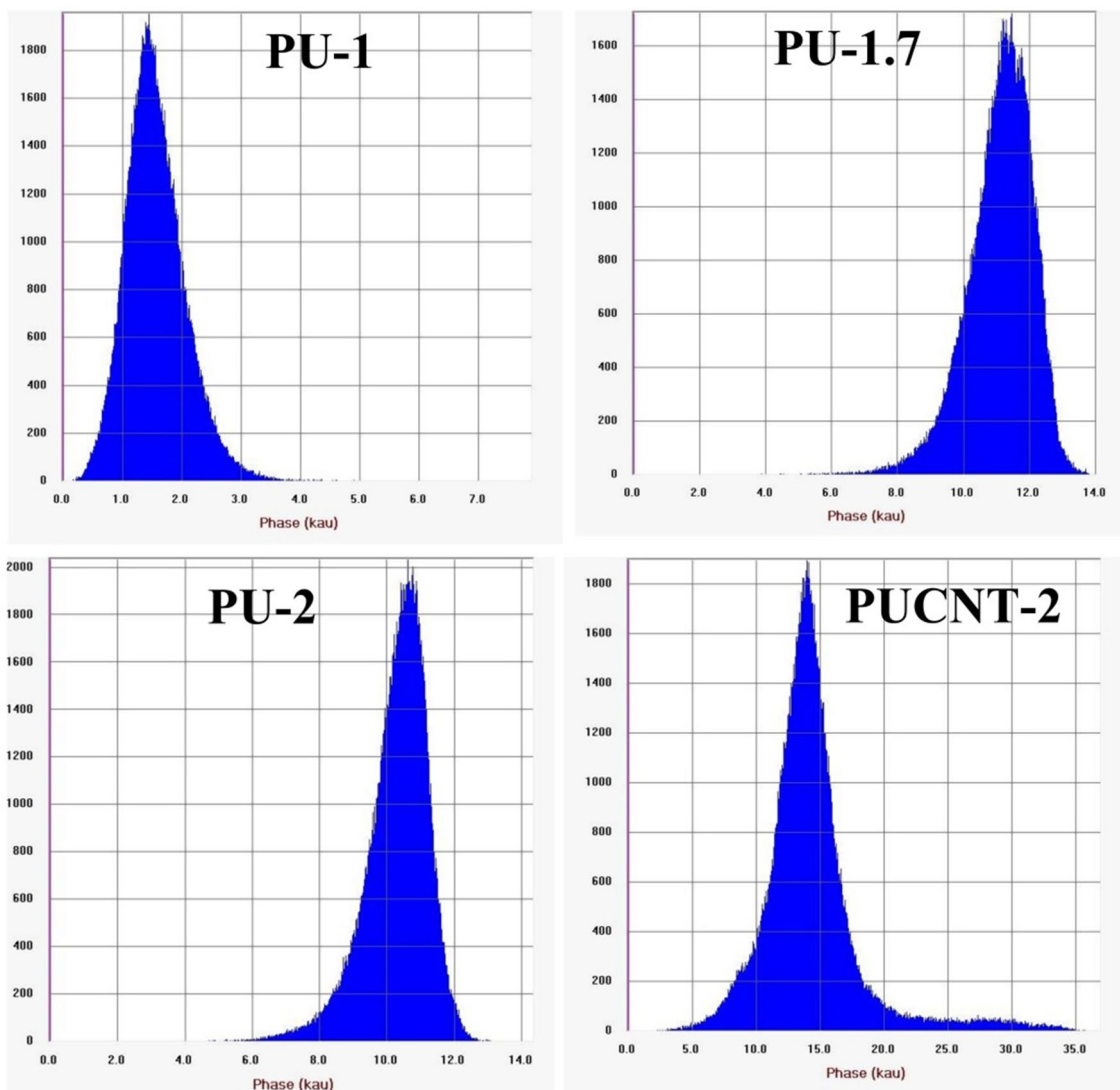


Fig. 14 AFM histograms of PU-1, PU-1.7, PU-2 and PUCNT-2 nanocomposites

hindrance effect is more important in the earlier stages due to the induced thermoplastic character. However, as the reaction proceeds, the reinforcing effect of CNTs is progressively growing due to the formation of interactions between CNTs and urethane groups of PU chains. All in all, it could be rationally stated that the reinforcing effect is the most dominant in the case of PUCNT-2, which is the major reason for the observed boost in mechanical properties for this sample comparing with PUCNT-1.7.

Conclusions

The PUs and PU-CNT nanocomposites with different NCO/OH molar ratios were synthesized from a polyester diol derived from waste PET bottles. The observed

results according to FTIR analysis, mechanical, dynamic mechanical and morphology tests were in a good agreement with each other. The chemical shifts of the urethane groups in FTIR, which represent the strength of hydrogen bonding, the Young's modulus, storage modulus, Tg and hardness strength of samples, were in the same order of: PUCNT-2 > PU-1.7 > PU-2 > PUCNT-1.7 > PU-1. Such trend was ascribed to the effects of NCO/OH molar ratio and addition of CNT. Introduction of CNT caused formation of a powder-like material in NCO/OH molar ratio of 1, and opposing effects (steric hindrance and reinforcing) were observed for samples with NCO/OH molar ratio 1.7 and 2, respectively. Adhesion factor showed a reduction for PUCNT-2 ($A = -0.038$) as compared with PUCNT-1.7 ($A = 0.333$). An increased phase separation for the synthesized PU in NCO/OH of 1.7 during the post-curing process

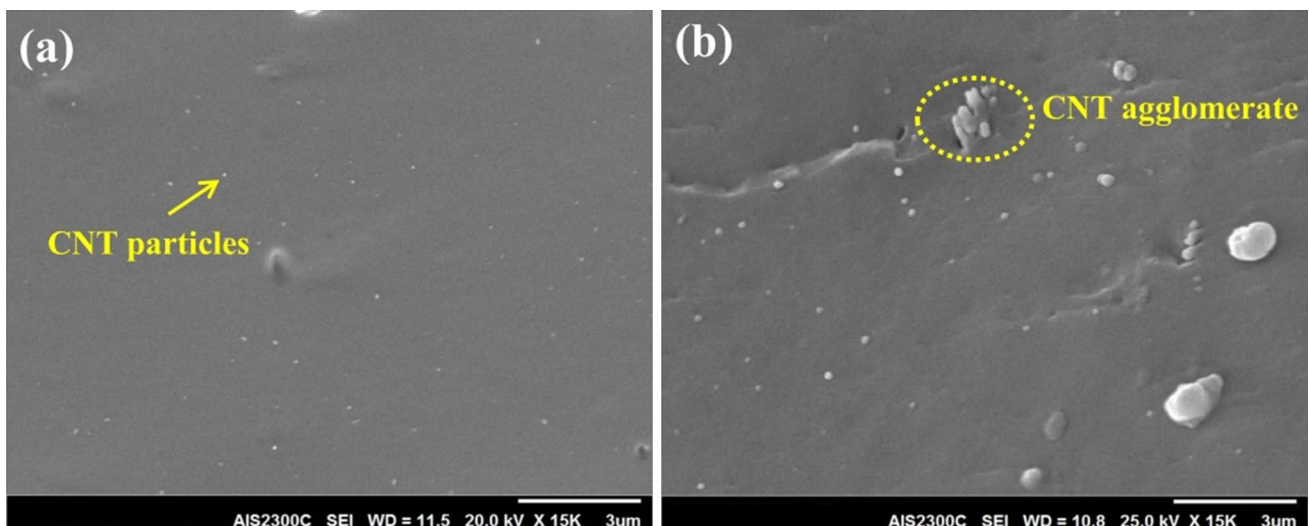


Fig. 15 SEM images of: **a** PUCNT-1.7, and **b** PUCNT-2 nanocomposites

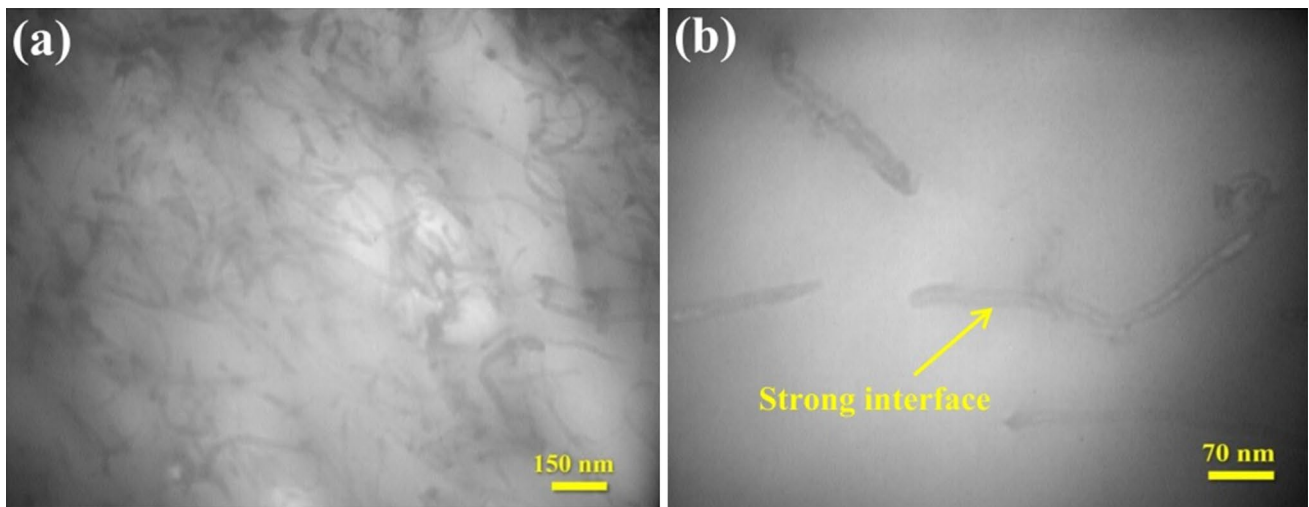


Fig. 16 TEM images of PUCNT-2 nanocomposite

led to enhanced CLD, mechanical and dynamic mechanical parameters as compared to those of 2 and 1. Several methods were utilized to measure CLD values of the PUs and PU/CNT nanocomposites. The obtained CLD values were in the following order: $\nu_E > \nu_{MR} > \nu_{DMA} > \nu_{SW} > \nu_{GR}$. From the knowledge of the CLD calculated by the Young's modulus, Mooney–Rivlin, rubbery plateau region in DMTA curve, strain hardening modulus and swelling, it was possible to determine the individual contributions of the three types of crosslinks (chemical, permanent, and temporary physical

entanglements). During abrasion test, the applied shear stress caused the CNTs to be withdrawn from the polymer matrix resulting in creation of voids and cracks, and thus, the abrasion resistance was reduced for the nanocomposites as compared with their corresponding polyurethanes. Eventually, a mechanism was also proposed to further explicate the opposing effects of CNTs in the polymerization reaction and their overall influence on the final character of synthesized PU nanocomposites.

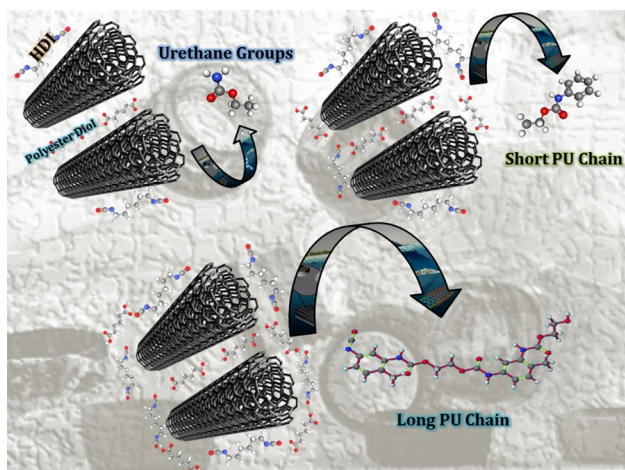


Fig. 17 Schematic representation of the proposed mechanism for the effect of CNTs on the polymerization reaction

References

- Rastin H, Ahmadi Z, Pakdel AS, Saeb MR, Abbasian Y, Liravi M, Eslahi A (2016) *J Vinyl Addit Technol* 22:387
- Al-Salem S, Lettieri P, Baeyens J (2009) *Waste Manage* 29:2625
- Abdolmaleki M, Tavakoli T, Jazani OM, Saeb MR (2016) *J Polym Eng* 36:513
- Luo X, Li Y (2014) *J Polym Environ* 22:318
- Jazani OM, Arefazar A, Peymanfar MR, Saeb MR, Talaei A, Bahadori B (2013) *Polym Plast Technol Eng* 52:1295
- Haghdadeh P, Ghaffari M, Ramezanzadeh B, Bahlakeh G, Saeb MR (2018) *J Taiwan Inst Chem Eng* 86:199
- Formela K, Hejna A, Zedler Ł, Przybysz M, Ryl J, Saeb MR, Piszczczyk Ł (2017) *Ind Crops Prod* 108:844
- Colomines G, Rivas F, Lacoste ML, Robin JJ (2005) *Macromol Mater Eng* 290:710
- Lee SC, Sze YW, Lin CC (1995) *J Appl Polym Sci* 55:1271
- Shamsi R, Abdouss M, Sadeghi GMM, Taromi FA (2009) *Polym Int* 58:22
- Sadeghi GMM, Shamsi R, Sayaf M (2011) *J Polym Environ* 19:522
- Shamsi R, Sadeghi GMM (2016) *RSC Adv* 6:38399
- Shamsi R, Mir Mohamad Sadeghi G, Asghari GH (2016) *Polym Compos.* <https://doi.org/10.1002/pc.24155>
- Hadavand BS, Najafi F, Saeb MR, Malekian A (2017) *High Perform Polym* 29:651
- Zedler Ł, Colom X, Saeb MR, Formela K (2018) *Compos B* 145:182
- Atieh MA, Bakather OY, Al-Tawbini B, Bukhari AA, Abui-laiwi FA, Fettouhi MB (2011) *Bioinorg Chem Appl.* <https://doi.org/10.1155/2010/603978>
- Rastin H, Ahmadi Z, Saeb MR, Formela K (2016) *J Vinyl Add Tech* 22:415
- Najafi F, Bakhshandeh E, Hadavand BS, Saeb MR (2014) *Prog Org Coat* 77:1957
- Vahabi H, Gholami F, Karaseva V, Laoutid F, Mangin R, Sonnier R, Saeb MR (2017) *Prog Org Coat* 113:207
- Halvaei M, Didehban K, Goodarzi V, Ghaffari M, Ehsani M, Saeb MR (2017) *J Appl Polym Sci* 134:45389. <https://doi.org/10.1002/app.45389>
- de Paiva JMF, Frollini E (2006) *Macromol Mater Eng* 291:405
- Kaddami H, Dufresne A, Khelifi B, Bendahou A, Taourirte M, Raihane M, Issartel N, Sautereau H, Gerard J-F, Sami N (2006) *Compos A Appl Sci Manuf* 37:1413
- Pothan LA, Oommen Z, Thomas S (2003) *Compos Sci Technol* 63:283
- Pothan LA, Thomas S, Groeninckx G (2006) *Compos A Appl Sci Manuf* 37:1260
- Ahankari S, Kar KK (2008) *Mater Sci Eng, A* 491:454
- Amrollahi M, Sadeghi GMM, Kashcooli Y (2011) *Mater Des* 32:3933
- Barick A, Tripathy D (2010) *Mater Sci Eng A* 527:812
- Van Melick H, Govaert L, Meijer H (2003) *Polymer* 44:2493
- Sari MG, Vahabi H, Gabrion X, Laheurte P, Zarrintaj P, Formela K, Saeb MR (2018) *Prog Org Coat* 119:171
- Sari MG, Saeb MR, Shabanian M, Khaleghi M, Vahabi H, Vagner C, Zarrintaj P, Khalili R, Paran SMR, Ramezanzadeh B (2018) *Prog Org Coat* 115:143
- Bakhshandeh E, Jannesari A, Ranjbar Z, Sobhani S, Saeb MR (2014) *Prog Org Coat* 77:1169
- Formela K, Klein M, Colom X, Saeb MR (2016) *Polym Degrad Stab* 125:1

Publisher's Note Springer Nature remains neutral with regard to jurisdictional claims in published maps and institutional affiliations.